Final Technical Report

Grant Number: DE-FG02-05ER46228

Awarded to: University of Wisconsin, Milwaukee

Principal Investigator: Lian Li

Co-principal Investigator: Michael Weinert

Period Covered: 07/15/2005 - 12/31/2016

DOE/Office of Science Program Office: Electron and Scanning Probe Microscopies, Division of Materials Sciences and Engineering

DOE/Office of Science Program Manager: Dr. Jane Zhu

Date: March 8, 2017

Our BES supported program integrates molecular beam epitaxy (MBE) growth with *in situ* atomic scale imaging using scanning tunneling microscopy/spectroscopy (STM/STS) and atomic force microscopy (AFM). Aided by density functional theory (DFT) calculations, we explore enhanced functionalities emerging from the interplay of strain, proximity, and spin-orbit interactions in heterostructures of wide band gap semiconductors, graphene, and Dirac materials, focusing on three thrusts: 1) doping wide bandgap semiconductors and graphene; 2) graphene nanoribbons and graphene-semiconductor heterostructures; and 3) Dirac materials. Our findings and discoveries have led to the publication of one book chapter and twenty-three refereed journal articles, including several in high impact journals: three Nature Communications, two Physical Review Letters, One Nano Letters, and one ACS Nano. Highlights of each thrust are provided below.

1ST THRUST: DOPING WIDE BANDGAP SEMICONDUCTORS AND GRAPHENE

In this thrust, we focused on the doping of semiconductor and graphene in the search for homogeneous high temperature diluted magnetic semiconductors (DMS), addressing two fundamental questions: 1) how are dopant- or defect-induced local moments created in semiconductors, and 2) how do these moments interact with each other to attain long range ferromagnetic ordering. DMS are generally made by doping semiconductors with transition metals, since magnetism is typically associated with elements that have partially filled *d* and *f* shells. To this end, we have investigated the MBE growth of GaN thin films, and discovered an autosurfactant effect during GaN MBE (*Phys. Rev. Lett.* ***98****, 206106 (2007)*). We have further characterized the structural and magnetic properties of Mn/GaN system by spin-polarized STM using Fe coated W tips, and demonstrated atomically resolved spin-dependent imaging on Mn_xGa_{1-x}/GaN(0001) (*Phys. Rev. B* ***80****, 235323 (2009*)).

- ***An atomistic view of the autosurfactant effect during GaN epitaxy***

Because of the considerable difference in atomic radii of group III (Ga, In, and Al) elements and N, and more importantly the large binding energy of the N_2 molecule, nitride surfaces terminated with group-III adlayers are more energetically favorable. These metal-rich surfaces can impact the epitaxial growth of nitrides favorably, since the excess metal atoms on top of the growing surface can serve as surfactant during growth, modifying the growth kinetics from diffusion-limited to that of exchange-limited. In this work, we investigate the Ga-N site-exchange, a critical process of the autosurfactant effect during epitaxial growth of GaN. On the GaN(0001) pseudo (1x1) surface, we find that the presence of two Ga adlayers instigates two Ga-N site exchanges for the N adatoms before their incorporation and the formation of a new GaN bilayer. The first site-exchange results in N incorporation at the subsurface T_1 site between the top and second Ga layer, forming metastable layer. The second exchange that converts the layer to that of bilayer-height can be triggered by continued STM imaging, which is driven by electrostatic force induced by electrons tunneling to or from localized states associated with the second layer Ga. This sets off a chain reaction which frees these Ga atoms, allowing N to form covalent Ga-N-Ga bond of a new GaN bilayer. These results provide the first atomistic view of the autosurfactant effect of Ga during MBE growth of GaN (*Phys, Rev. Lett.* ***98****, 206106 (2007)*).

- ***Standing waves on GaN(0001)***

In this work, we have applied Fourier Transform STM (FT-STM) to investigate standing waves on the GaN(0001)-pseudo (1x1) metallic surface, which consists of two atomic Ga layers with the top layer incommensurate. Two types of periodic oscillations are observed at room

temperature. The longer wavelength standing waves are due to electron scattering by dislocation-induced steps and deposited two-dimensional InN islands. The localized shorter wavelength waves are attributed to a structural transition of the incommensurate Ga bilayer to a tetrahedral Ga bilayer after the growth of InN islands. This work has been published in *Nanotechnol.* ***21****, 435401 (2010)* as a cover article.

- ***Defect-induced magnetism in graphene***

Localized defect states in *s* and *p* shell materials can also lead to local moments and cause these materials to exhibit ferromagnetism. To explore this novel effect, we have investigated *defect-induced magnetism* in graphene, a one-atom-thick planar sheet of sp^2-bonded carbon atoms densely packed in a honeycomb lattice, exhibiting a linear band dispersion near the K points, as described by the same equations as two-dimensional massless Dirac fermions. As such, graphene exhibits exotic physical and electronic properties such as a room temperature Quantum Hall effect, and extremely high electron mobility, which has been explored for practical applications, e.g., a 100 GHz graphene transistor was recently fabricated.

The promise of graphene, however, can extend far beyond. While magnetism is typically associated with the *d*- and *f*-shell materials such as iron, magnetic moments can also be created by localized states of a vacancy in graphene, leading to *magnetism without magnetic ions*, which can be further tailored by substitutional doping or adsorption of molecules. Our work indicates that because of the very strong in-plane σ bonds that form the backbone of its honeycomb lattice, doping graphene requires the assistance of high-energy ions of insert gases (e.g., nitrogen plasma), which produces impurity-vacancy complexes (e.g., N-vacancy).

In this part of the research, we first determined the atomic structure of the 1st graphene layer grown on 6H-SiC(0001), a critical but controversial issue in the epitaxial growth of graphene. We then carried out atomic resolution imaging of various vacancy defects using non-contact AFM, and made the first determination of their charge by local contact potential measurements using site specific force-bias df/dU spectroscopy. We further determined the role of N in vacancy-induced magnetism in graphene. Highlights of these discoveries are provided below.

- ***The role of functionalized transition-metal coated W tips in STM imaging: Application to epitaxial graphene on SiC(0001)***

W tips functionalized by Fe and Cr coating are typically used in spin-polarized STM. Here, the densities for majority and minority spins for Cr and Fe coated tips at various biases were calculated, which indicate that spatial extent and character of the majority and minority states differ, as expected since they are derived from exchange split bands. The tip polarization, $(n_\uparrow - n_\downarrow)/(n_\uparrow + n_\downarrow)$, integrated over the separation plane, varies with bias voltage in the range of 10-30%, which sets an approximate upper bound for the polarization achievable with these tips. Interestingly, the polarization can switch sign with bias; for example, the polarization of Fe empty states (used to image filled sample states) switches from +7% for a bias of 0.25 eV to -8% for 0.5 eV. Because of the difference between the majority and minority states, the two spin

directions of the tip have inherently different imaging resolutions. This work has been published in *Phys. Rev. B* ***84****, 125425 (2011))*.

- ***Discovery of a new warped interface structure in epitaxial graphene on SiC(0001)***

In this work, we have shown that epitaxial graphene growth on Si-face SiC(0001) starts with the formation of a warped interfacial layer with periodic inclusions of pentagon-hexagon-heptagon ($H_{5,6,7}$) complexes within the honeycomb lattice. The $H_{5,6,7}$ regions deviate locally from the honeycomb lattice of ideal graphene, relieving strain between the graphene layer and the SiC substrate, while still retaining the three-fold coordination for each carbon atom and providing local commensurability with the substrate. During the subsequent growth, the interfacial layer remains to be $H_{5,6,7}$, while the succeeding layers assume the usual graphene honeycomb lattice. The model explains the consistencies and variation in the structural and electronic properties of the epitaxial graphene/SiC(0001), ending the decades-long controversy on the nature of its interface. This work has been published in *Phys. Rev. Lett.* [24] and a book chapter in *"Physics and Applications of Graphene: Experiments"* (http://www.intechopen.com/articles/show/title/epitaxial-graphene-on-sic-0001-more-than-just-honeycombs). The $H_{5,6,7}$ complex, the key feature of the interfacial graphene structure, was also featured as the logo for the 70th Physical Electronic Conference in 2010, as shown on the right.

The discovery of the warped interfacial structure between graphene and SiC(0001) was made possible by STM investigation using W tips functionalized with Fe and Cr coating, which enables the selective imaging of states within a few meV of the Fermi level that are not accessible with conventional W tips, where imaging is typically limited to ~1-2 eV above or below the Fermi level. By modeling these tips using X/W(110) (X=Cr, Fe, W) slabs by DFT calculations, we found that this selectivity is due to the enhanced tunneling from states located ~0.4-0.6 eV above and below E_F for the Fe/W tips, and 0.3 eV above E_F for the Cr/W tips. Furthermore, we found that the formation of an apex atom is not stable for W/W(110) or Fe/W(110) tips, but is stable for Cr/W(110) tips. This apex atom results in point-like iso-density of states contours for Cr/W tips.

- ***Measuring graphene vacancy charge states by atomic force microscopy***

In this work, we have carried out atomic resolution imaging of various vacancy defects using noncontact-AFM, and made the first determination of their charge by local contact potential measurements using site specific force-bias df/dU spectroscopy. While the df-dU spectrum of neutral graphene away from the defects exhibits the expected parabolic shape with a maximum at -0.6 eV, a shift of this maxima towards more positive (-0.572 eV) and negative (-0.654 eV) values for the defects that are negatively and positively charged, respectively. To further ascertain the presence of these charges at these two type of vacancy defects, z-dependent measurements were also performed at different heights above the surface. For the neutral graphene, a relatively constant value of the parabolic maxima is obtained within the range of *z* measured. For defects, however, while the same constant values are measured away from the

defects (where the impact of the charges on the local contact potential is negligible), progressively larger deflection towards opposite directions are observed as the tip is moved closer to the surface, consistent with oppositely charged defects.

These observations are in excellent agreement with density functional theory calculations, where single, di-, and multi-vacancy complexes are found to be positively charged, while H adsorbates at these vacancy defects can produce negatively charged structures. These results provide new insights into charge states of vacancy defects in graphene, and their tunability by size and doping. These findings have been published in *Nanotechnol.* ***26****, 215702 (2015)* as a cover article.

- ***Magnetism of nitrogen doped epitaxial graphene on SiC(0001)***

The removal of one carbon atom from graphene creates the simplest defect: a vacancy. As a result, localized states are created around the vacancy, leading to a magnetic moment of 0.84 μ_B. Furthermore, our calculations also show that the presence and precise position of a single N atom near a carbon vacancy in graphene can have profound effects on the spin configurations of the system. We found that the vacancy-induced magnetic moments can be enhanced by the presence of nitrogen nearby the vacancy. In addition, the net magnetic moment varies with not only the presence of N, but also its relative distance from the vacancy. For example, in the configuration where the N positioned at the nearest site to the vacancy, no net magnetic moment is found. In configurations where the N atom and vacancy are further apart, a localized magnetic moment is found, similar to that of the vacancy-only case, however with an enhanced net magnetic moment of 1.09 μ_B. These results indicate that the engineering of complexes of vacancy defects and impurities may provide a unique way to enhance the magnetism in graphene.

We have experimentally confirmed that nitrogen doping of epitaxial graphene on SiC(0001) leads to the formation of N-vacancy complexes. Based on the calculated energetics and comparisons with STM observations, we find that the most probable configuration is a nonmagnetic single vacancy with a substitutional nitrogen at the nearest neighbor site, a motif that also serves as the building block for various other N-vacancy complexes. These findings are published in *Appl. Phys. Lett.* ***100****, 233119 (2012).*

2ND THRUST: GRAPHENE NANORIBBONS AND GRAPHENE-SEMICONDUCTOR HETEROJUNCTIONS

In this thrust, we have fabricated and demonstrated tunable bandgaps in semiconducting zigzag nanoribbons with hydrogen edge termination by Fe nanoparticle assisted etching of epitaxial graphene. We have synthesized hydrogen-terminated zigzag semiconducting variant as small as 1 nm in width, and observed spin polarized edge states. We further discovered a threshold of 3 nm for the onset of the electron-electron correction that's key to the gap opening, and have measured a gap of 1.6 eV for 1 nm ribbon, largest found so far. In addition, metallicity is also observed in oxygen-terminated zigzag nanoribbons. We have shown that fluctuations in Schottky barrier height at the graphene-semiconductor (SiC, Si, and GaAs) junctions are directly

related to the spatial and charge density variations in the graphene layer. Highlights of these discoveries are provided below.

- ***Nano ridges on graphene/ SiC(0001)***

Epitaxial graphene is compressively strained due to the mismatch of its lattice and thermal coefficient with the SiC substrate. While strain in bulk materials is typically relieved through the formation of dislocations, a 2D material such as graphene that possesses strong in-plane covalent bonding and weak interlayer interaction is free to buckle and bend away from the substrate to form ridges. In this work, using atomic resolution STM imaging, we revealed that the ridges are indeed the bulged regions of the graphene layer. In addition, we found that it is possible to manipulate these ridges, and even create new ones during STM imaging. By using vicinal SiC substrates, where terrace sizes are much smaller and the compressive strain is minimized, we have grown near ridge-free graphene films. This work has been published in the *Nanotechnol.**20**, 355701 (2009)* as a cover article.

- ***Semiconducting graphene zigzag nanoribbons with H-termination***

While pristine graphene is a semimetal with linear dispersion at the Dirac point, graphene nanoribbons provide new functionalities, such as tunable energy gap and spin-polarized edge states. In this part of the research, we have fabricated H-terminated zigzag nanoribbons using Fe nanoparticles assisted etching of epitaxial graphene/SiC(0001) in hydrogen. Nanoribbons as small as 1 nm can be made using this method as shown in the STM image below.

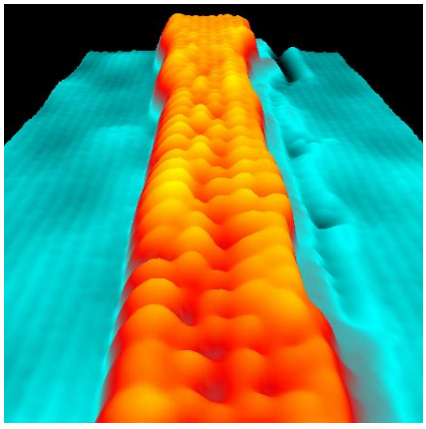

We find two gaps in their local density of states by tunneling spectroscopy. In addition, the gaps are found to be strongly dependent on their width. For ribbons wider than 3 nm, gaps up to 0.39 eV are found independent of their width (w), consistent with DFT calculations. For ribbons narrower than 3 nm, however, much larger gaps are obtained, which also scale inversely with w, supporting the need for quasiparticle corrections to the calculated gap. A 1.6 eV gap is found for a 1 nm ribbon. These results provide the first direct experimental confirmation of electron-electron interactions in the gap opening of graphene zigzag nanoribbons, and reveal a critical width of 3 nm for the onset of such interactions.

The finding of a critical threshold for the onset of the quasiparticle electron-electron correction to the gap for narrower ribbons is fully consistent with the fact that the interior of wider ribbons (>5 nm) are nominally graphene, a zero gap semiconductor. Therefore, quasiparticle corrections to the gap are not relevant since there is no gap to begin with. This work has been published in *Nat. Commun. **5**, 4311 (2014).*

- ***Schottky barrier fluctuations at graphene-semiconductor junctions***

When interfaced with a semiconductor, graphene forms a Schottky junction with rectifying properties. Different than a conventional metal/semiconductor junction, the Schottky barrier height at the graphene/semiconductor is simply the difference between their work functions. Owing to the lack of interface states at the nonbonding graphene/semiconductor junction, and the readily tunable graphene Fermi level, the barrier height can be directly controlled by an electric field. These Schottky contacts offer platforms for interesting physics, as well as practical applications in a variety of electronic devices, most notably three terminal transistors that have led to an on/off ratio of 10^5.

Unique also to graphene, a 2D material with a negative coefficient of thermal expansion, is that it is susceptible to deformation when interfaced with another material or under an electric field. In this part of the research, we investigated the effect of these graphene "ripples" on the Schottky barrier height at graphene/semiconductor junctions. Our work reveals two intrinsic atomic-scale inhomogeneities: topographic ripples and electron-hole puddles that cause Schottky barrier height fluctuations. Because graphene is just one atomic layer thick, spatial inhomogeneities are inherent and are known to the graphene community. However, our work is the first to relate atomic scale fluctuations to transport measurements of Schottky barrier height that controls carrier transport in graphene/semiconductor junctions.

Experimentally, chemical vapor deposited graphene is transferred onto semiconductor substrates, as confirmed by Raman spectroscopy and STM imaging. Tunneling spectroscopy indicates that for graphene/C-SiC, the Dirac point is at 0.42 eV below E_F, while on the Si-face it is 0.35 eV above, a direct consequence of the larger work function at the Si-face. In addition, we observe spatial fluctuations in the Schottky barrier height caused by the intrinsic rippling at the graphene/SiC interface. The spatial variation of the Dirac energy directly follows the undulation of the ripples, exhibiting a Gaussian distribution with a full-width-at-hall-maximum of 42 and 51 meV for graphene transferred on C- and Si-SiC, respectively, consistent with calculations. This result reflects an intrinsic effect inherent for graphene/semiconductor Schottky contacts, and has been published in *Nat. Commun.* ***4****, 2752 (2013).*

- ***Transport measurements of spatial fluctuations of barrier height at graphene/semiconductor Schottky junctions***

In this part of research, intrinsic spatial inhomogeneity in barrier height at graphene/SiC, GaAs and Si Schottky junctions was investigated using transport measurements. Temperature dependent I-V measurements clearly show rectifying behaviors. Nevertheless, we find that non-ideal behavior such as an increase of zero bias Schottky barrier height and decrease of ideality factor with increasing temperature is directly related to the three main types of spatial inhomogeneities as revealed by STM: atomic scale ripples, nanometer ridges, and deformation caused by SiC steps. Using the modified thermionic emission model, assuming a Gaussian distribution of the barrier, mean Schottky barrier heights of 1.30±0.18 eV and 1.16±0.16 eV are found for graphene/SiC junctions on the C- and Si-face, respectively. These findings are the first transport study of how the spatial inhomogeneities at graphene/semiconductor junctions directly impact its Schottky barrier height. The results on graphene/SiC have been published in *Appl. Phys. Lett.* ***105****, 021607 (2014).* Similarly for graphene/Si and GaAs junctions, mean Schottky barrier heights of 1.14±0.14 and 0.76±0.10 eV are found. In these cases, barrier inhomogeneities are attributed to interfacial states (*Nanotechnol.* ***26****, 215702 (2015)).*

3RD THRUST: DIRAC MATERIALS

The focus of this thrust is Dirac materials, particularly topological insulator (TI) where the low energy excitations responsible for electronic and optical transport are described by effective Dirac equations for massless fermions. We are particularly interested in the symmetry protected boundary states that are robust against perturbations that do not break the symmetry, offering exciting opportunities in fundamental physics and potential applications such as energy efficient computation and energy conversion. Highlights of the discoveries are provided below.

- ***Revealing the origin of the linear dispersion of silicene/Ag(111)***

Silicene and germanene, the silicon and germanium 2-D analogues of graphene, are predicted to have linearly dispersing Dirac states at the Fermi level, and can be potentially compatible with existing semiconductor processing technology. In contrast to carbon in graphene, however, both silicon and germanium favor sp^3 bonding rather than sp^2. This preference is manifested in the predicted buckled honeycomb structures for the isolated systems that are essentially (111) bilayers of the bulk materials. Thus, while atomically thin unsupported sheets of graphene are stable and can be transferred rather easily, substrates appear to be required to stabilize silicene and germanene.

In this part of the research, we have theoretically investigated the impact of the Ag(111) substrate on the band structure of the newly discovered silicene, an Si analog of graphene. A k-projection technique that includes the k_z-dependence of the surface bands is used to separate the contributions arising from the silicene and the Ag substrate, and to "unfold" the supercell band structure. The bands for both the clean Ag(111) substrate and the interacting system show that there is an intense state arising from the bottom of the bulk Ag sp band that crosses the Fermi level near the K point of the (1x1) silicene. For the silicone/Ag(111) case, a comparison of the dispersion and intensity of bands with those of the Ag(111) surface indicates that the observed linear band is predominately derived from the substrate.

This approach allows for a consistent comparison between the calculations and the angle-resolved photoemission experiments, including the photon (k_z) dependence. Our calculations reproduce the observed gap and linear dispersion across the K point of silicene, but demonstrate that this originates from the Ag(111) substrate and is not a Dirac state. This work has been published in *Nano Letters* ***14****, 5189 (2014)*.

- ***Gapped Dirac cone in silicene and germanene on Al_2O_3(0001)***

In order to minimize the effect of the substrate on their electronic properties, our calculations show that wide band gap inert materials are promising candidates. The interaction of silicene (and germanene) with this class of substrates is discussed below, focusing on Al_2O_3(0001). The calculated low energy structure of $\sqrt{13}$x$\sqrt{13}$ silicene on a 3x3 Al_2O_3(0001) is reconstructed, consisting of both high- and low-buckled Si atoms. The binding energy is reduced compared to silicene on Ag(111), but is still sizable (~0.52 eV/Si), indicating that the interaction is not simply van der Waals. The band alignment for Al-terminated Al_2O_3(0001) and silicene places the Dirac point of isolated silicene in the middle of the gap, and suggesting no charge transfer or direct interaction between substrate states and the silicene Dirac states. (For oxygen-terminated surface, the silicene Dirac point is also in the gap, but closer to the top.)

Next, we calculated the electronic states for both an isolated silicene layer with the same reconstructed structure and the interacting system. Despite the reconstruction, the isolated

silicene bands are very similar to that of the ideal silicene, particularly for the valence bands. The reconstruction breaks symmetry, leading to the opening of a small gap (~0.1 eV) at the Dirac point, although the dispersion of the valence Dirac bands remains almost linear away from K. The changes are more significant for the interacting case: (i) the σ bands below -5 eV are heavily modified, indicating interactions with the substrate; (ii) the valence (and conduction) π bands are broken up by minigaps; (iii) the gap at K is increased to 0.44 eV; and (iv) the dispersion around the Dirac point is no longer a cone, but rather consists of sections of almost flat bands. These modifications in the electronic bands occur in absence of substrate states in the same energy region, and is a result of indirect interactions via deeper lying states. For other less energetically favorable structural configurations (e.g., with a Si directly above an oxygen site), the bands form a gapped Dirac cone around K.

For germanene we find significantly different behaviors for metallic and semiconducting substrates. For germanene on Au(111) with an almost flat honeycomb lattice, the electronic interactions with the substrate are so strong that the isolated germanene features become indistinguishable. For Al_2O_3 substrate, on the other hand, germanene effectively maintains the ideal low-buckled structure, along with approximately linear dispersion of the Dirac states and a small gap. These results demonstrate the sensitivity of the electronic states of silicene and germanene to substrate interactions, and suggest pathways to tune their electronic properties. These findings have been published in *Phys. Rev. B* ***94****, 075409 (2016).*

- ***Electrical detection of spin-momentum locking in Dirac and Rashba states***

Three-dimensional TIs exhibit time-reversal symmetry protected Dirac surface states, which are occupied by a single spin and exhibit helical spin-momentum locking. In the two-dimensional electron gas (2DEG) with a parabolic energy dispersion, the Rashba form of spin-orbit coupling (SOC) also leads to a pair of Fermi surfaces that exhibit counter-rotating chiral spin texture, locking spin to the linear momentum. As such, an unpolarized bias current is predicted to create a net spin polarization due to the spin-momentum locking in both systems. In collaborations Naval Research Laboratory, spin potentiometric measurements of bias current-generated spin polarization were carried out in Bi_2Se_3(111) films where Dirac surface states coexist with normal 2DEG states, and on InAs(001) samples where only normal 2DEG states are present. Spin polarization arising from spin-momentum locking are observed in both cases, with opposite signs of the spin voltage. A model based on spin dependent electrochemical potentials is also developed to directly derive the signs expected for the TI surface states, and unambiguously show that the dominant contribution to the current-generated spin polarization measured in the TI is from the Dirac surface states.

This work provides the first direct comparison of the helical spin texture of Dirac and Rashba 2DEG states through electrical transport measurements. This direct electrical access of the helical spin texture of Dirac and Rashba 2DEG states is an enabling step toward the development of TI and SOC-based spintronics and energy efficient computation and information storage. These results have been published in *Nat. Commun.* ***7****, 13518 (2016).*

- ***Revealing novel indirect interlayer bonding mechanism in graphene / topological insulator van der Waals heterostructures***

With spin-orbit coupling opening a gap at the Dirac point, graphene also exhibits a second type of edge state, making it a quantum spin Hall insulator, i.e., 2D topological insulator. However, due to its intrinsically small spin-orbit interaction, the observation of these edge states

is exceedingly challenging. To enhance the spin-orbit coupling, the obvious solution of doping is often not a viable one because of the accompanying structural (and electronic) changes induced. Other proposals involving periodic arrangement of transition metal atoms on graphene are not only challenging to achieve experimentally, but also introduces scattering centers that reduces graphene mobility.

A more promising approach to enhance the SO interaction in graphene would be via proximity effect where other modifications to graphene is minimal. We synthesized a prototypical van der Waals (vdW) heterojunction by transferring chemical vapor deposited graphene onto topological insulator Bi_2Se_3 grown by MBE. Using STM/S, we demonstrate a giant spin-orbit splitting of the graphene Dirac states up to 80 meV (compared to intrinsic values of 24-50 ueV), with a spatial variation of ±20 meV. Density functional calculations show that this splitting is a result of the proximity to Bi_2Se_3, which breaks the inversion and horizontal mirror symmetries of the graphene, thus lifting the four-fold degeneracy of its bands at the Dirac point. Furthermore, the transfer of the spin-orbit coupling is found to be through Bi character introduced into the graphene Dirac states due to orthogonalization to the Bi_2Se_3 states. Moreover, we find that the strong spatial fluctuation in the transferred SOC in graphene is due to the inherent non-epitaxial relation at the graphene / Bi_2Se_3 interface.

Our results demonstrate an enhancement of several orders of magnitude of the spin splitting of the graphene Dirac bands. They further reveal two intrinsic characteristics – the symmetry breaking and orthogonalization of the wave functions at the interface – that underlines the properties in vdW heterostructures. Our findings indicate that albeit weakly bonded, new properties and functionalities not present for the constituent 2D layers nevertheless emerge in vdW heterostructures. Without direct covalent bonding at the interface, these properties arise from mechanisms of unconventional nature. These results have been published in *ACS Nano **10**, 8450 (2016)*.

A list of book chapters:

1. "Epitaxial graphene on SiC(0001): More than just honeycombs", L. Li, book chapter in "*Graphene, Theory, Research and Applications*" (http://www.intechopen.com/books/show/title/physics-and-applications-of-graphene-experiments).

A list of referred journal publications:

1. "Observation of standing waves at steps on GaN(0001) pseudo-(1x1) surface by scanning tunneling spectroscopy at room temperature", M. L. Harland and L. Li, *Appl. Phys. Lett. **89**, 132104 (2006)*.
2. "Atomistic view of the autosurfactant effect during GaN epitaxy", S. T. King, M. Weinert, and L. Li, *Phys. Rev. Lett. **98**, 206106 (2007).*
3. "Incorporation of Ge on GaN(0001), Y. Qi, S. T. King, S. H. Cheng, M. Weinert, L. Li, *Appl. Phys. Lett. **92**, 111918 (2008).*
4. (*Cover article*) "Atomic-scale imaging and manipulation of ridges on epitaxial graphene on 6H-SiC(0001)", G. F. Sun, J. F. Jia, Q. K. Xue, and L Li, *Nanotechnol. **20,** 355701 (2009).*
5. "Electronic structures of Mn-induced phases on GaN(0001)", Y. Qi, G. F. Sun, M. Weinert, and L. Li, *Phys. Rev. B **80**, 235323 (2009).*

6. "Epitaxial graphene on SiC(0001): More than just honeycombs", Y. Qi, S. H. Rhim, M. Weinert, and L. Li, *Phys. Rev. Lett.* **105**, 085502 (2010).
7. (*Cover article*) "Electron standing waves on the GaN(0001)-pseudo (1 × 1) surface: a FT-STM study at room temperature", G. F. Sun, Y. Liu, Y. Qi, J. F. Jia, Q. K. Xue, and M. Weinert, and L Li, *Nanotechnol.* ***21,*** *435401 (2010).*
8. "A novel Si diffusion path for pit-free graphene growth on SiC(0001)", G. F. Sun, S. H. Rhim, Y. Liu, Y. Qi, J. F. Jia, Q. K. Xue, M. Weinert, and L. Li, *Phys. Rev. B* ***84****, 195455 (2011).*
9. "Role of functionalized transition-metal coated W tips in STM imaging: Application to epitaxial graphene on SiC(0001)", S. H. Rhim, Y. Qi, G. F. Sun, Y. Liu, M. Weinert, and L. Li, *Phys. Rev. B 84, 125425 (2011).*
10. "Formation of nitrogen-vacancy complexes during plasma-assisted nitrogen doping of epitaxial graphene on SiC(0001)", S. H. Rhim, Y. Qi, Y. Liu, M. Weinert, and L. Li, *Appl. Phys. Lett.* ***100****, 233119 (2012).*
11. "Spatial fluctuations in barrier height at the graphene-SiC Schottky contact", S. Rajput, M. X. Chen, Y. Y. Li, Y. Liu, M. Weinert, and L. Li, *Nat. Commun.* ***4****, 2752 (2013).*
12. "Direct experimental evidence for the reversal of carrier type upon hydrogen intercalation in epitaxial graphene/SiC(0001)", S. Rajput, Y. Y. Li, and L. Li, *Appl. Phys. Lett.* ***104****, 041908 (2014).*
13. "Direct experimental determination of onset of electron-electron interactions in gap opening of zigzag graphene nanoribbons", Y. Y. Li, M. X. Chen, M. Weinert, and L. Li, *Nat. Commun.* ***5****, 4311 (2014).*
14. "Intrinsic inhomogeneity in barrier height at monolayer graphene/SiC Schottky junction", D. Tomer, S. Rajput, L. J. Hudy, C. H. Li, and L. Li, *Appl. Phys. Lett.* ***105****, 021607 (2014).*
15. "Transport and photoconduction characteristics of metal-graphene-4H-SiC(0001) heterojunction devices", T. Hosseini, D. Tomer, S. Rajput, L. Li, and N. Kouklin, *Appl. Phys. Lett.* ***105****, 223107 (2014).*
16. "Revealing the substrate origin of the linear dispersion of silicene/Ag(111). M. X. Chen and M. Weinert, *Nano Lett.* ***14****, 5189 (2014).*
17. "Determining charge state of graphene vacancy by noncontact atomic force microscopy and first-principles calculations", Y. Liu, M. Weinert, and L. Li, *Nanotechnol.* ***26****, 035702 (2015).*
18. "Carrier transport in reverse-biased graphene/semiconductor Schottky junctions", D. Tomer, S. Rajput, L. J. Hudy, C. H. Li, and L. Li, *Appl. Phys.* ***106****, 173510 (2015).*
19. "Inhomogeneity in barrier height at graphene/Si (GaAs) Schottky junctions", D. Tomer, S. Rajput, L. J. Hudy, C. H. Li and L. Li, *Nanotechnol.* ***26****, 215702 (2015).*
20. "Designing substrates for silicene and germanene: First-principles calculations", M. X. Chen, M. Weinert, and Z. Zhong, *Phys. Rev. B* ***94****, 075409 (2016).*
21. "Half-metallic Dirac cone in zigzag graphene nanoribbons on graphene", M. X. Chen and M. Weinert, *Phys. Rev. B* ***94****, 035433 (2016).*
22. "Direct comparison of current-induced spin polarization in topological insulator Bi_2Se_3 Dirac states and InAs Rashba states", C. H. Li, O. M. J. van 't Erve, S. Rajput, L. Li, and B. T. Jonker, *Nat. Commun.* ***7****, 13518 (2016).*

23. "Indirect interlayer bonding in graphene-topological insulator van der Waals heterostructure: giant spin-orbit splitting of the graphene Dirac states", S. Rajput, Y. Y. Li, M. Weinert, and L. Li, *ACS Nano* ***10****, 8450 (2016).*